Revision 3

New thermobarometers for martian igneous rocks, and some implications for secular cooling on Mars

Jerrod Lessel[1,*] and Keith Putirka[1]

[1]Department of Earth and Environmental Sciences, California State University, Fresno, Fresno, CA 93740, U.S.A. Address: 2576 E San Ramon Ave. M/S ST24, Fresno, CA, 93740 *E-mail: jlessel@iri.columbia.edu

Abstract

Tests show that terrestrial mineral+liquid geothermobarometers are not well equipped for use on martian rocks, which tend to have much higher FeO and lower Al_2O_3. Here, we present new calibrations of thermometers and barometers using experimental data on martian samples from the literature. These new models recover *P-T* conditions with a greater accuracy compared to models calibrated using terrestrial compositions. We applied these new calibrations to primitive martian mantle derived melts Yamato 980459 (Y98) and Northwest Africa (NWA) 6234 and several surface basalts (Gusev). Our new models yield similar *P-T* conditions for NWA and Y98 compositions of 1.4-1.7 GPa and 1500-1550 °C, which are close to estimates by most prior studies. Our models yield somewhat lower *P* estimates compared to Lee et al. (2009), apparently because our Si-activity model (from Beattie 1993) includes an Al_2O_3-correction (where lower Al_2O_3, as in martian samples, leads to lower *P* estimates). For Gusev basalt compositions, our new models yield *P-T* estimates of 1.0-1.3 GPa and 1340-1390 °C; furthermore, we also obtain $P = 1.03$ GPa and $T = 1340$ °C, for a Gusev composition from Monders et al. (2007), which comes very close to the Monders et al. (2007) estimate for multiple saturation, of 1.0 GPa and 1325 °C, derived from phase saturation relationships. Given the different ages of these meteorites, with Gusev at 3.65 Ga (Greeley et al. 2005) and Y98 at 4.3 Ga (Bouvier et al. 2005, 2008, 2009; Werner et

al. 2014), their thermal contrasts may represent secular cooling of Mars. We estimate a mantle potential temperature difference of ~200 °C, with mantle potential temperatures of 1450 ± 50 °C for Gusev and 1650 ± 50 °C for Y98; this implies a cooling rate of 300 °C/Ga. This would appear to be a much more rapid rate of cooling compared to Earth, as may be expected by Mars' higher surface/volume ratio.

Keywords: geothermobarometry, thermobarometry, martian meteorites, experimental petrology, martian geology, thermometer, barometer, Mars, petrology, SNC meteorites

Introduction

Geothermobarometers are useful tools as they lend insights into the inner workings of planetary bodies (see Essene, 1989; Brey and Köhler, 1990; Putirka et al., 1996; Putirka, 2008). This was illustrated during the Apollo era, when return samples from the Moon gave scientists unique opportunities to apply geothermobarometry to a planetary body other than Earth (see McCallum and Schwartz, 2001; Lee et al., 2009). For example, workers discerned lower to middle crustal depths of recrystallization and partial melting in lunar samples (McCallum and Schwartz, 2001), which bolstered arguments for convective overturn of the lunar mantle early in its history (Lee at al., 2009). However, as indicated by Filberto and Dasgupta (2011) and as we show below, thermobarometers calibrated on terrestrial compositions (Putirka et al. 1996; Putirka 2008) are poor predictors of *P* and *T* when applied to experiments performed on martian bulk compositions. We thus calibrate new thermometers and barometers that are specific to martin bulk compositions.

Martian meteorites

Martian meteorites are primarily comprised of basalts and basaltic cumulates (Shergottites), Ca-rich clinopyroxene cumulates (Nakhlites), and Dunites (Chassignites) in addition to other unique samples such as orthopyroxenite ALH84001 (Papike et al., 2009) and a porphyritic basaltic monomict breccia NWA7034 (Agee et al., 2013). Shergottites themselves are typically further subdivided into basaltic, lherzolitic, and olivine-phyric shergottites (Goodrich, 2002). Furthermore, the literature shows that martian bulk compositions are different from common terrestrial samples in a number of ways. For example, Papike et al. (2009) compared the bulk silicate compositions of Earth, Mars, the Moon, and Vesta (see Papike et al., 2009; their tables 5 and 6) and showed that martian basalts are enriched in FeO and depleted in Al_2O_3 when compared to terrestrial samples. Papike et al. (2009) estimated that average martian basaltic compositions for Al_2O_3 and FeO were 6.55 wt% and 18.0 wt% respectively. We show similar contrasts between the two rock types using total FeO (FeOt) in liquids from partial melting experiments on martian bulk compositions, with an average of 16.6 ± 4.29 wt% FeOt is compared to 8.60 ± 3.15 wt% FeOt when terrestrial bulk compositions are used (Fig. 1a). We also illustrate that liquids equilibrated from martian samples have less Al_2O_3, with an average 10.6 ± 3.12 wt% Al_2O_3 as compared to 14.8 ± 3.92 wt% Al_2O_3 for terrestrial basalts (Fig. 1b).

Since the bulk of martian meteorites are cumulates, there has been no pressing need for new mineral-liquid thermobarometers. But, with new martian rover and potential future sample return missions, accurate mineral-liquid thermometers and barometers are likely to prove quite useful for understanding martian magmatic processes. As we show

below, the contrasts between martian and terrestrial samples lead to problems when models calibrated using terrestrial samples are used to predict *P* and *T* for martian rocks. For example, when we applied a two-pyroxene barometer from Putirka (2008) to experimental martian meteorite data (n = 39), it obtained an R^2 value of 0.08, with a root mean square error (RMSE) of 0.62 GPa. We thus calibrate new thermometers, and barometers, following Putirka (2008), using equilibria that involve clinopyroxene (Cpx), orthopyroxene (Opx), and olivine (Ol).

Methodology

The models in this study follow the thermodynamic approach presented in Putirka (2008), where *P* and *T* are related to equilibrium compositions using an equilibrium constant (K_{eq}), which is in turn related to the Gibbs free energy of pure substances at a standard state ($\Delta G°$ in units of J/mole) through the familiar expression: $\Delta G° = -RT\ln K_{eq}$ (where *R* equals the gas constant J/K·mole and *T* is temperature in K). This equation can be expanded to derive equations that express *P* as a function of *T* and composition (see Putirka, 2008). Regression analyses are performed using JMP statistical software (SAS Institute Inc., 2010). Calculations of liquid and mineral components are as in Putirka (2008; Tables 1-3), where liquid components are treated as cation fractions. The pyroxene components were calculated using a normative scheme, as the cations are calculated on the basis of six oxygens (see examples in Putirka, 2008).

Experimental data collected from the literature span a wide array of *P*, *T*, and liquid compositions (Table 1); these data range from 1 atm to 2.3 GPa and 950-1540 °C, with liquid compositions covering 40.2-66.16 wt% SiO_2, 0.62-24.52 wt% MgO, 2.80-

30.2 wt% FeO, 2.97-20.5 wt% Al_2O_3, and 0.19-6.77 wt% total alkalis. The total number of data (n) for various equilibria are as follows: cpx+liquid, n=63; opx+liquid, n=89; ol+liquid, n=115. In each case, we use approximately 83% of the data for calibration and withhold 17% for use as test data. After testing various percentages, the ratio of calibration to test data was chosen to have a test data set large enough to verify accuracy, but still retain a calibration data set that included the widest possible range of liquid compositions and *P*-*T* conditions to produce precise models. In addition to mineral-liquid equilibria, we also calibrate 1) a two-pyroxene thermometer and barometer (n=39) and 2) a Si-Activity barometer (n=29), where 21% and 24% of the data are respectively reserved for test purposes. Because of the limited amount of total data for these models we increased the percentage of the test data sets to insure the accuracy of the models. Volatile bearing samples were used in the calibration and testing of the models and were treated the same as the other experimental data. Because of the sensitivity of the Ol+Liq thermometers to volatiles, figure 6 shows the distribution of hydrated data (from Dann et al. 2001, Filiberto 2008, and McCubbin et al., 2008) and Cl-rich data (from Filiberto and Treiman, 2009) used in the model. Experimental data on martian compositions are from: (Bertka and Holloway, 1989; Dann et al., 2001; Filberto, 2008; Filberto et al., 2008, 2009; Filberto and Treiman, 2009; Herd et al., 2002; Longhi and Pan, 1989; McCanta et al., 2004; McKay et al., 1986; McCoy and Lofgren, 1999; McCubbin et al., 2008; Medard and Grove, 2006; Minitti and Rutherford, 2000; Monders et al., 2007; Musselwhite et al., 2006; and Singletary and Grove, 2008).

New models

Equations (1) and (2) are calibrated using clinopyroxene-saturated partial melting experiments on martian bulk compositions; mineral and liquid components are calculated as in Putirka (2008):

(1)

$$P(GPa) = -412.7 + 9.667\times10^{-6}T(K)\ln\left[\frac{X_{Jd}^{cpx}}{X_{AlO_{1.5}}^{liq}\cdot X_{NaO_{0.5}}^{liq}\cdot (X_{SiO_2}^{liq})^2}\right] + 722.1[X_{SiO_2}^{liq}] + 5.496[X_{MgO}^{liq}] - 195.0\ln[X_{SiO_2}^{liq}] - 334.7[(X_{SiO_2}^{liq})^2] + 686.3[(X_{TiO_2}^{liq})^2] + 30.77[(X_{AlO_{1.5}}^{liq})^2] - 57.14[(X_{CaO}^{liq})^2]$$

The term X_{Jd}^{cpx} is equal to $X_{Al(VI)}^{cpx}$ or $X_{NaO0.5}^{cpx}$, whichever is less and if excess $X_{Al(VI)}^{cpx}$ remains then $X_{CaTs}^{cpx} = X_{Al(VI)}^{cpx} - X_{Jd}^{cpx}$ (from Putirka, 2008). Eqn. (1) reproduces *P* for the calibration data with an $R^2 = 0.91$ and an RMSE = ± 0.17 GPa, and predicts *P* for test data with $R^2 = 0.94$ and an RMSE of ± 0.22 GPa (Fig. 2).

(2)

$$\frac{1}{T(K)} = 7.463\times10^{-4} - 1.855\times10^{-5}\ln\left[\frac{X_{Jd}^{cpx}\cdot X_{CaO}^{liq}\cdot X_{Fm}^{liq}}{X_{DiHd}^{cpx}\cdot X_{NaO_{0.5}}^{liq}\cdot X_{AlO_{1.5}}^{liq}}\right] - 7.417\times10^{-4}\left[X_{TiO_2}^{liq}\right] + 1.981\times10^{-4}\left[X_{AlO_{1.5}}^{liq}\right] - 9.346\times10^{-4}\left[X_{MgO}^{liq}\right] - 6.891\times10^{-4}\left[X_{NaO_{0.5}}^{liq}\right] + 1.605\times10^{-3}\left[X_{CrCaTs}^{cpx}\right]$$

Eqn. (2) is based on the Jadeite–Diopside/Hedenbergite exchange equilibrium presented in Putirka et al., 1996. In Eqn. (2), the terms $X_{CrCaTs}^{cpx} = X_{CrO1.5}^{cpx}/2$; $X_{DiHd}^{cpx} = (X_{CaO}^{cpx} - [X_{Al(IV)}^{cpx} - X_{CaTs}^{cpx}]/2 - X_{CaTs}^{cpx} - X_{CrCaTs}^{cpx})$; and $X_{Fm}^{liq} = X_{FeO}^{liq} + X_{MgO}^{liq}$. The calibration data for Eqn. (2) recovered *T* with an $R^2 = 0.96$ and an RMSE of ± 22 K, while *T* for the test data was predicted with $R^2 = 0.90$ and an RMSE of ± 41 K (Fig. 3).

The next set of models is based on orthopyroxene-liquid equilibria.

This is a preprint, the final version is subject to change, of the American Mineralogist (MSA)
Cite as Authors (Year) Title. American Mineralogist, in press.
(DOI will not work until issue is live.) DOI: http://dx.doi.org/10.2138/am-2015-4732

(3)

$$P(GPa) = -5.050 + 35.05\left[X_{TiO_2}^{liq}\right] + 6.458\left[X_{AlO_{1.5}}^{liq}\right] - 10.67\left[X_{CaO}^{liq}\right] + 1.438\left[Mg\#^{liq}\right] - 20.74\left[X_{TiO_2}^{opx}\right] - 6.188\left[X_{AlO_{1.5}}^{opx}\right] + 0.01915\left[D_{MgO}^{opx/liq}\right] + 1.111\left[\frac{X_{AlO_{1.5}}^{opx}}{X_{AlO_{1.5}}^{liq}} + \frac{X_{NaO_{0.5}}^{opx}}{X_{NaO_{0.5}}^{liq}} + \frac{X_{SiO_2}^{opx}}{X_{SiO_2}^{liq}}\right]$$

(4)

$$\frac{1}{T(K)} = 2.234\times10^{-4} - 3.982\times10^{-6}\left[D_{MgO}^{opx/liq}\right] - 9.394\times10^{-4}\left[X_{NaO_{0.5}}^{opx}\right] - 2.058\times10^{-4}\ln\left[X_{MgO}^{liq}\right] + 3.564\times10^{-5}\ln\left[X_{CaO}^{liq}\right] + 2.186\times10^{-4}\ln\left[X_{MgO}^{opx}\right] - 1.958\times10^{-5}\ln\left[X_{Al(IV)}^{opx}\right] + 0.002298\left[X_{Al(IV)}^{opx}\right]^2$$

In the orthopyroxene-liquid models the term $D_{MgO}^{opx/liq} = X_{MgO}^{opx}/X_{MgO}^{liq}$ and the term $X_{Al(IV)}^{opx} = 2 - X_{SiO2}^{opx}$. In Eqn. (3), *P* is recovered for the calibration data with R^2 = 0.89 and an RMSE = ± 0.20 GPa, while *P* is predicted for test data with R^2 = 0.91 and RMSE = ± 0.21 GPa (Fig. 4). Equation (4) reproduces *T* for calibration data with an R^2 = 0.94 and RMSE = ± 33 K, while *T* is predicted for test data with R^2 = 0.96 and an RMSE = ± 27 K (Fig. 5).

We also calibrate a thermometer based on olivine + liquid equilibria.

(5)

$$\frac{1}{T(K)} = 6.529\times10^{-4} - 6.425\times10^{-4}\left[X_{TiO_2}^{liq}\right] - 1.049\times10^{-3}\left[X_{MgO}^{liq}\right] - 4.206\times10^{-5}\ln\left[X_{FeO}^{liq}\right] - 4.121\times10^{-5}\ln\left[X_{NaO_{0.5}}^{liq}\right] + 2.047\times10^{-3}\left[X_{NaO_{0.5}}^{liq}\right]^2 - 8.807\times10^{-4}\left[X_{SiO_2}^{ol}\right]^2 + 2.299\times10^{-6}\left[D_{MgO}^{ol/liq}\right]$$

where $D_{MgO}^{ol/liq} = X_{MgO}^{ol}/X_{MgO}^{liq}$. In Eqn. (5) the calibration data are reproduced with R^2 = 0.88 and an RMSE = ± 48 K, while *T* for the test data is predicted with R^2 = 0.90 and an RMSE = ± 38 K (Fig. 6). Because many martian samples appear to be cumulates, we also calibrate a two-pyroxene thermometer and barometer, with components calculated as in Putirka (2008):

(6)

$$P(GPa) = -3.764 + 0.6739[X_{CaO}^{cpx}] + 33.45[X_{Jd}^{cpx}] + 4.033[X_{DiHd}^{cpx}] - 5.945[X_{Di}^{opx}] + 3.320\left[\frac{X_{EnFs}^{cpx}}{X_{Fm_2Si_2O_6}^{opx}}\right] + 40.34[X_{AlO_{1.5}}^{cpx} \cdot X_{AlO_{1.5}}^{opx}] - 75.80[(X_{AlO_{1.5}}^{cpx} \cdot X_{NaO_{0.5}}^{cpx}) + (X_{AlO_{1.5}}^{opx} \cdot X_{NaO_{0.5}}^{opx})]$$

(7)

$$\frac{1}{T(K)} = 6.644\times10^{-4} - 2.757\times10^{-5}[P(GPa)] + 1.499\times10^{-3}\left[X_{NaO_{0.5}}^{opx}\right] - 1.640\times10^{-4}\left[X_{Fe^{2+}}^{cpx}\right] + 6.664\times10^{-5}\left[X_{DiHd}^{cpx}\right]^2 + 2.611\times10^{-4}\left[X_{FeO}^{opx}\right]^2 - 6.602\times10^{-8}\left[\frac{1}{X_{CaTs}^{cpx}}\right] + 6.869\times10^{-8}\left[\frac{1}{X_{NaO_{0.5}}^{opx}}\right] - 1.166\times10^{-8}\left[\frac{1}{X_{FmAl_2SiO_6}^{opx}}\right]$$

The parameter $X_{Fe2+}^{cpx} = X_{FeO}^{cpx} - X_{Fe3+}^{cpx}$ where the term X_{Fe3+}^{cpx} is based on the calculation from Papike et al. (1974) and is calculated as: $X_{Fe3+}^{cpx} = X_{Al(IV)}^{cpx} + X_{NaO0.5}^{cpx} - X_{Al(VI)}^{cpx} - X_{CrO1.5}^{cpx} - 2X_{TiO2}^{cpx}$. Equation (6) reproduced *P* for the calibration data with R^2 = 0.93 and RMSE = ± 0.17 GPa, while *P* is predicted for test data with R^2 = 0.96 and an RMSE = ± 0.16 GPa (Fig. 7). In Eqn. (7) the calibration data are reproduced with R^2 = 0.99 and an RMSE = ± 12 K, while *T* for the test data are predicted with R^2 = 0.95 and an RMSE = ± 37 K (Fig. 8).

The Si-activity barometer uses the liquid components in which only ol and opx have formed (see Putirka, 2008).

(8)

$$P(GPa) = -11.16 - 184.3[X_{MnO}^{liq}] - 5.268[X_{MgO}^{liq}] + 21.18[a_{SiO_2}^{liq}] + 4.961[X_{NaO_{0.5}}^{liq} + X_{KO_{0.5}}^{liq}] - 3.577 \times 10^{-3} T(K) \ln[a_{SiO_2}^{liq}]$$

In Eqn. (8), the activity of SiO_2 is calculated from Beattie (1993): $a_{SiO2}^{liq} = (3X_{SiO2}^{liq})^{-2} \cdot (1-X_{AlO1.5}^{liq})^{7/2} \cdot (1-X_{TiO2}^{liq})^{7}$; the calibration data are reproduced with $R^2 = 0.91$ and RMSE = ± 0.16 GPa , while *P* is predicted for the test data with $R^2 = 0.92$ and an RMSE = ± 0.18 (Fig. 9).

Fe-Mg Exchange Equilibria and Tests of Equilibrium

As a test of inter-phase equilibrium, we consider one of the classic means of evaluation, the Fe-Mg exchange coefficient as established by Roeder and Emslie (1970):

(9)

$$K_D(Fe\text{-}Mg)^{min\text{-}liq} = [X_{FeO}/X_{MgO}]^{mineral}/[X_{FeO}/X_{MgO}]^{liquid}$$

where X_i are mole fractions of FeO or MgO in a silicate liquid (liq) and a co-existing silicate mineral (min). This equilibrium constant is known from prior studies to be slightly sensitive to *T*, *P*, and composition (e.g., Longhi et al. 1978; Herzberg and O'Hara 1998; Toplis 2005; Matzen et al., 2011), but such variations are quite small and over limited compositional and *P*-*T* ranges, this equilibrium constant is independent of such variables. It thus provides an important and useful means for establishing whether a given ferromagnesian silicate mineral is in equilibrium with a putative liquid composition.

Like Filiberto and Dasgupta (2011) we find that the equilibrium constant describing Fe-Mg exchange between olivine and liquid, $K_D(Fe\text{-}Mg)^{ol\text{-}liq}$ (Roeder and Emslie, 1970), is significantly higher for martian than terrestrial systems (Filiberto and Dasgupta, 2011 found a $K_D(Fe\text{-}Mg)^{ol\text{-}liq} = 0.35 \pm 0.01$), and it is also sensitive to the model used to calculate F_2O_3/FeO in a liquid when fO_2 is given. We calculated $K_D(Fe\text{-}Mg)^{ol\text{-}liq}$ using Kress and Carmichael (1988), Kress and Carmichael (1991; Eqns. 6 and 7), Borisov (2010) and Jayasuria et al. (2004; Eqn. 12). We obtained a low and a high for the mean $K_D(Fe\text{-}Mg)^{ol\text{-}liq}$ for martian samples using Kress and Carmichael (1991; Eqn. 7), which yields $K_D(Fe\text{-}Mg)^{ol\text{-}liq} = 0.366 \pm 0.023$ and Jayasuria et al. (2004; Eqn. 12), which produces $K_D(Fe\text{-}Mg)^{ol\text{-}liq} = 0.385 \pm 030$ (n=95). Experiments by Filiberto (2008) yield liquids with unusually high K_2O contents compared to other martian silicate liquids, but even removing these, the mean $K_D(Fe\text{-}Mg)^{ol\text{-}liq}$ values are 0.363 ± 0.023 and 0.383 ± 0.03 using the Kress and Carmichael (1991) and Jayasuria et al. (2004) models respectively.

We use the Kress and Carmichael (1991; Eqn. 7) model for all calculations of Fe_2O_3/FeO in experimental liquids. Absent the high K_2O samples, we find that $K_D(Fe\text{-}Mg)^{ol\text{-}liq}$ values are quite nearly independent of melt composition, *P* and *T*. We obtain a slight positive dependence of the $K_D(Fe\text{-}Mg)^{ol\text{-}liq}$ on Ti:

(10)

$$K_D(Fe\text{-}Mg)^{ol\text{-}liq} = 0.356 + 0.012[TiO_2 \text{ wt. } \%]^{liquid}.$$

But this equation captures <5% of the total variation of $K_D(Fe\text{-}Mg)^{ol\text{-}liq}$ ($R^2 = 0.03$), so for practical purposes, $K_D(Fe\text{-}Mg)^{ol\text{-}liq}$ may be considered a constant and a useful test of equilibrium. Ignoring compositional effects, we recommend an equilibrium value of

(11)

$K_D(Fe\text{-}Mg)^{ol\text{-}liq} = 0.36 \pm 0.02.$

Unlike $K_D(Fe\text{-}Mg)^{ol\text{-}liq}$, the coefficient for orthopyroxene + liquid equilibrium, $K_D(Fe\text{-}Mg)^{opx\text{-}liq}$, is much more sensitive to liquid composition. The global mean is $K_D(Fe\text{-}Mg)^{opx\text{-}liq} = 0.303 \pm 0.010$. But variations in K_2O account for 30-45% or more of the variation of $K_D(Fe\text{-}Mg)^{opx\text{-}liq}$ (depending upon which data are excluded from the regression), and so we do not recommend that the mean value be used as a test of equilibrium. Instead, it is best to use:

(12)

$$K_D(Fe\text{-}Mg)^{opx\text{-}liq} = 0.32 - 0.05[K_2O^{liq}\ \text{wt. \%}]^{liquid}$$

where $R^2 = 0.45$, the standard error of estimate (SEE) = ± 0.03, and we use the Kress and Carmichael (1991; Eqn. 7) model to calculate Fe_2O_3/FeO in the silicate liquid. After accounting for this compositional effect, no other compositional parameter, nor *P* and *T*, describes more than 3% of remaining variation in $K_D(Fe\text{-}Mg)^{opx\text{-}liq}$.

Interestingly, values for $K_D(Fe\text{-}Mg)^{cpx\text{-}liq}$ for martian clinopyroxene-liquid pairs are rather close to their terrestrial counterparts, with a mean of about 0.26 ± 0.05. However, like orthopyroxene, $K_D(Fe\text{-}Mg)^{cpx\text{-}liq}$ is also sensitive to alkali content:

(13)

$$K_D(Fe\text{-}Mg)^{cpx\text{-}liq} = 0.32 - 0.02[Na_2O + K_2O^{liq}\ (\text{wt. \%})]^{liquid}.$$

where $K_D(Fe\text{-}Mg)^{cpx\text{-}liq}$ is calculated using Fe_2O_3/FeO ratios in the liquid from Kress and Carmichael (1991: Eqn. 7). This model explains ~30% of the variation of $K_D(Fe\text{-}Mg)^{cpx\text{-}liq}$, and the SEE = ±0.03, when those samples falling further than 3σ away from the mean

(n = 43) are excluded.

Finally, we calibrate an Fe-Mg exchange coefficient for clinopyroxene and orthopyroxene:

(14)

$$K_D(\text{Fe-Mg})^{\text{cpx-opx}} = [X_{FeO}/X_{MgO}]^{\text{cpx}}/[X_{FeO}/X_{MgO}]^{\text{opx}}$$

The global mean is $K_D(\text{Fe-Mg})^{\text{cpx-opx}} = 0.942 \pm 0.144$, but as might be expected from the mineral-liquid exchange equilibria, this coefficient is sensitive to composition. In this case, however, the compositional effects appear to be a proxy for a somewhat stronger thermal variation. While it would be more thermodynamically correct to use a regression equation of the form $\ln K = f(1/T)$, this empirical relationship describes a slightly greater fraction of the variation:

(15)

$$K_D(\text{Fe-Mg})^{\text{cpx-opx}} = 0.115 + 7.693\text{x } 10^{-4}[T(^{\circ}\text{C})]$$

where $R^2 = 0.44$ and SEE = ± 0.09 (n = 38). We do not recommend this as a "weak" thermometer but instead $K_D(\text{Fe-Mg})^{\text{cpx-opx}}$ can be used as a check in the application of a geothermometeric result. As a *T*-independent test, the following compositionally dependent model may be more useful:

(16)

$$K_D(\text{Fe-Mg})^{\text{cpx-opx}} = 1.262 - 0.023[\text{CaO (wt.\%)}]^{\text{cpx}}$$

where the CaO content of clinopyroxene serves as a proxy for *T* and the model explains about 30% of the variation amongst 39 experimental data, with an SEE of ± 0.10.

Comparisons of the new mineral+liquid models

Table 2 shows the regression statistics of the new models compared with those in table 3 that shows the statistics for models from Putirka et al. (1996) and Putirka (2008), when using martian compositions to predict *T* or *P*. This comparison highlights the result that the new models yield lower errors and better precision. For example, the new cpx-liq barometer (Eqn. 1) predicts a *P* for martian samples with half the error (± 0.22 GPa) compared to Eqn. 32a from Putirka (2008; ± 0.40 GPa). The increased precision is even greater for orthopyroxene-liquid equilibria, and the new models are significantly more precise for each of the equilibria examined.

Discussion and Implications

Yamato 980459 (Y98) is one of the few martian meteorites that is thought to represent a primitive mantle derived melt (Lee et al., 2009; Filiberto and Dasgupta, 2011) along with Northwest Africa (NWA) 6234 (Gross et al., 2013). Y98 is most similar to the olivine-phyric shergottites, although it lacks plagioclase (likely due to the presence of glassy mesostasis) and has highly magnesian mineral components (Mikouchi et al., 2004). Dalton et al. (2005) described Y98 compositionally as comprised of 48% pyroxene, 26% olivine, 25% mesostasis, and 1% other minerals. Y98 is thought to represent a primitive martian magma derived from a highly reduced mantle (Mikouchi et al., 2004). Indeed, Y98's olivine composition has the highest MgO of any of the martian meteorites (Fo_{84}) and so Y98 appears to be the most primitive martian magma found to date (Dalton et al. 2005, 2007). NWA 6234 is also an olivine-phyric shergottite, with olivine crystals set in a finer grained groundmass of pyroxene, maskelynite, and accessory minerals (Filiberto et al., 2012; Gross et al., 2013). NWA 6234 is unique

among the olivine-phyric shergottites because it is the only one thought to be from a primitive ferroan magma with a source region located deeper than other martian basalts (Gross et al., 2013). As a test, we apply our new calibrations to Y98 and NWA 6234.

Presented here are only the *P*-*T* estimates of mineral-liquid pairs for Y98 and NWA 6234 that passed our tests of equilibrium. When calculating pressures and temperatures for Y98, the Si-activity barometer (Eqn. 8) was combined with the olivine thermometer (Eqn. 5) and a simple empirical MgO thermometer:

$$T(^{o}C) = 1011 + 29.8[\text{MgO wt. \%}] \; . \qquad (17)$$

A $K_D(\text{Fe-Mg})^{\text{ol-liq}}$ for Y98 was determined by pairing the "bulk chemistry for Y 980459" composition (used as the liquid component) from Greshake et al.'s (2004) table 6 with the "olivine core" composition (Fo_{84}), the highest Fo olivine from their Table 3. This olivine-whole rock pair yields a $K_D(\text{Fe-Mg})^{\text{ol-liq}}$ of 0.40 at QFM-3 (Herd, 2006) and a temperature in the range of 1400-1500 °C, well above the expected value of 0.36 from, Eqn. 10. At $K_D = 0.36$, the equilibrium olivine would be Fo_{87}, and Eqn. 4 from Putirka et al. (2007) and this study's Eqn. 8 together yield a *T* of 1476 °C and *P* = 1.15 GPa (and a nearly identical *T* of 1480°C is obtained using Beattie, 1993). Our Eqn. 17 yields a *T* of 1550 °C but this *T* is probably too high given the more precise model of Putirka et al. (2007). For NWA 6234, if the whole rock is a liquid, then it would precipitate olivine of Fo_{85} composition, with $K_D = 0.37$, and at *T*-*P* conditions of 1499 °C and 1.34 GPa, using the same models as applied to Y98.

As shown in Figure 10 our new *P*-*T* estimates for Y98 are similar to those of prior studies: Blinova and Herd, 2009 (1.35 GPa and 1460 °C) and just slightly lower than

293 estimated by Musselwhite et al., 2006 (1.2 GPa and 1540 °C), but while our *T* estimates
294 are similar to Lee et al. (2009) we obtain a significantly lower *P* compared to their
295 estimate of 1.7 GPa. We attribute our lower *P* estimate to the use of an Al-activity
296 modifying term in the Beattie (1993) Si-activity model; the Lee et al. (2009) model lacks
297 such a term, and the inclusion of such yields lower pressure estimates as Al_2O_3 decreases.
298 For NWA 6234, our models lower *T* conditions from Gross et al., 2013 (1600 °C).
299 However, our *P* estimates are significantly lower than the *P* estimate from Gross et al.
300 (2013), who obtained a $P = 2.7$ GPa by applying the models of Putirka (2005) and Lee et
301 al. (2009). As with Y98, we suspect that the Al-activity term in the Beattie (1993) Si-
302 activity expression, which we use in our Eqn. (8), is responsible for this difference.
303 We also examined martian surface basalt compositions. Filberto (2011) also
304 found that martian surface basalts have a larger range of bulk compositions than the
305 shergottites, and the Gusev "recalibrated" composition reported by Monders et al. (2007)
306 is of special interest. Monders et al. (2007) show that this composition is multiply
307 saturated at 1 GPa and 1325 °C. Our Eqn. Si-activity barometer paired with Beattie
308 (1993) or Putrika et al. (2007; Eqn. 4) yields a higher *T* estimate of 1381 °C with a *P*
309 estimate of 1.33 GPa for this composition; while the *T* estimate is higher, the *P* estimate
310 is well within model error. But our simpler (although less precise) Eqn. (17), when
311 combined with our Si-activity barometer, comes remarkably close to their reported
312 conditions, with a *P*-*T* estimate of 1.1 GPa and 1340 °C, both within 1σ error of the
313 reported values. We thus tentatively conclude that Eqn. (17) might prove to be useful,
314 perhaps especially at lower temperatures.

These results support the idea that two different mantle processes (acting at different *P-T* conditions), rather than shallow level magma processing, are responsible for generating the meteorite and surface basalt populations. If this were the case, the Y98 source would appear to be characterized by olivines with distinctly higher Fo content (Fo_{84}), while the remaining basalts (including the NWA source, even though it yields similar *P-T* conditions compared to Y98) would have sources characterized by olivines with Fo_{80} compositions. Another possibility is that the surface-derived compositions are fractionated. It is not a necessary condition that multiply saturated basalts are mantle-derived, but if our pressure estimates (ca. 1 GPa) are accurate then that would imply that the crust must be >85 km thick, which has been suggested by others (see Gross et al., 2011). The other possibility, as noted by Monders et al. (2007) is that the martian mantle contains a range of mantle compositions, unhomogenized by mantle convection, which would be quite different from Earth, where sub-oceanic basalts converge to $Fo_{91.5}$, regardless of whether they derive from mantle plume or spreading ridge localities (Putirka et al., 2011). In any case, we obtain mantle potential temperatures of 1450 ± 50 °C at Gusev and 1650 ± 50 °C for Y98 (depending upon melt fraction which we assume is between 0.2 and 0.4). These estimates may have bearing on martain secular cooling rates. The Gusev samples are estimated to be 3.65 Ga (Greeley et al. 2005). In contrast, there has been some controversy regarding the age dates of Y98 and other shergottites, but new evidence appears to indicate an age ~4.3 Ga for this meteorite and shergottites generally (Bouvier et al. 2005, 2008, 2009; Werner et al. 2014). If we accept these ages, then the implied cooling rate is ~300 °C/Ga (≈ 200 °C/[4.3Ga -3.65Ga]), which is a much

faster rate than what is inferred for Earth (Herzberg et al. 2010) but perhaps reasonable given Mars' much greater surface-area-to-volume ratio.

Acknowledgements

We thank John Wakabayashi and Robert Dundas for their input and reviews of earlier drafts of this manuscript, and we thank J. Brian Balta, J Gross, and C. Herd for very thoughtful formal reviews of the present paper. J. Lessel thanks his wife, family, friends, and the entire CSU Fresno faculty for their support.

References cited

Agee, C. B., Wilson, N. V., McCubbin, F. M., Ziegler, K., Polyak, V. J., Sharp, Z. D., ... and Elardo, S. M. (2013). Unique meteorite from early Amazonian Mars: Water-rich basaltic breccia Northwest Africa 7034. Science, 339, 780-785.

Albarede, F. (1992). How deep do common basaltic magmas form and differentiate? Journal of Geophysical Research: Solid Earth (1978–2012), 97, 10997-11009.

Beattie, P. (1993). Olivine-melt and orthopyroxene-melt equilibria. Contributions to Mineralogy and Petrology, 115, 103-111.

Bertka, C. M., and Holloway, J. R. (1989). Martian Mantle Primary Melts: an Experimental Study of Melt Density and Viscosity and Viscosity at 23 KB. In Lunar and Planetary Institute Science Conference Abstracts, 20, 69.

359 Blinova, A., and Herd, C. D. (2009). Experimental study of polybaric REE partitioning
360 between olivine, pyroxene and melt of the Yamato 980459 composition: Insights into the
361 petrogenesis of depleted shergottites. Geochimica et Cosmochimica Acta, 73, 3471-3492.
362
363 Borisov, A. A. (2010). Ferric-ferrous ratio in liquid iron oxides: Analysis and
364 applications to natural basaltic melts. Petrology, 18, 471-481.
365
366 Bouvier, A., Blichert-Toft, J., Vervoort, J. D., and Albarède, F. (2005). The age of SNC
367 meteorites and the antiquity of the Martian surface. Earth and Planetary Science
368 Letters, 240, 221-233.
369
370 Bouvier, A., Blichert-Toft, J., Vervoort, J. D., Gillet, P., & Albarède, F. (2008). The case
371 for old basaltic shergottites. Earth and Planetary Science Letters, 266, 105-124.
372
373 Bouvier, A., Blichert-Toft, J., & Albarede, F. (2009). Martian meteorite chronology and
374 the evolution of the interior of Mars. Earth and Planetary Science Letters, 280, 285-295.
375
376 Brey, G. P., and Köhler, T. (1990). Geothermobarometry in four-phase lherzolites II.
377 New thermobarometers, and practical assessment of existing thermobarometers. Journal
378 of Petrology, 31, 1353-1378.
379
380 Bulatov, V. K., Girnis, A. V., and Brey, G. P. (2002). Experimental melting of a modally
381 heterogeneous mantle. Mineralogy and Petrology, 75, 131-152.
382

383 Dalton, H. A., Musselwhite, D. S., Kiefer, W. S., and Treiman, A. H. (2005).
384 Experimental petrology of the basaltic shergottite Yamato 980459: implications for the
385 thermal structure of the Martian mantle. Lunar and Planetary Institute Science
386 Conference, 36, 2142.
387
388 Dalton, H. A., Sharp, T. G., and Holloway, J. R. (2007). Investigation of the effects of
389 water on a Martian mantle composition. Lunar and Planetary Institute Science
390 Conference, 38, 2102.
391
392 Dann, J. C., Holzheid, A. H., Grove, T. L., and McSween, H. Y. (2001). Phase equilibria
393 of the Shergotty meteorite: Constraints on pre-eruptive water contents of martian magmas
394 and fractional crystallization under hydrous conditions. Meteoritics & Planetary
395 Science, 36, 793-806.
396
397 Draper, D. S., and Green, T. H. (1997). P–T phase relations of silicic, alkaline, aluminous
398 mantle-xenolith glasses under anhydrous and C–O–H fluid-saturated conditions. Journal
399 of Petrology, 38, 1187-1224.
400
401 Draper, D. S., and Green, T. H. (1999). P–T phase relations of silicic, alkaline, aluminous
402 liquids: new results and applications to mantle melting and metasomatism. Earth and
403 Planetary Science Letters, 170, 255-268.
404
405 Draper, D. S., and Johnston, A. D. (1992). Anhydrous PT phase relations of an Aleutian
406 high-MgO basalt: an investigation of the role of olivine-liquid reaction in the generation
407 of arc high-alumina basalts. Contributions to Mineralogy and Petrology, 112, 501-519.

Dunn, T., and Sen, C. (1994). Mineral/matrix partition coefficients for orthopyroxene, plagioclase, and olivine in basaltic to andesitic systems: a combined analytical and experimental study. Geochimica et Cosmochimica Acta, 58, 717-733.

Elkins-Tanton, L. T., Draper, D. S., Agee, C. B., Jewell, J., Thorpe, A., and Hess, P. C. (2007). The last lavas erupted during the main phase of the Siberian flood volcanic province: results from experimental petrology. Contributions to Mineralogy and Petrology, 153, 191-209.

Elkins-Tanton, L. T., and Grove, T. L. (2003). Evidence for deep melting of hydrous metasomatized mantle: Pliocene high-potassium magmas from the Sierra Nevadas. Journal of Geophysical Research, 108, 2350.

Essene, E. J. (1989). The current status of thermobarometry in metamorphic rocks. Geological Society, London, Special Publications, 43, 1-44.

Falloon, T. J., Danyushevsky, L. V., and Green, D. H. (2001). Peridotite melting at 1 GPa: reversal experiments on partial melt compositions produced by peridotite–basalt sandwich experiments. Journal of Petrology, 42, 2363-2390.

Falloon, T. J., Green, D. H., Danyushevsky, L. V., and Faul, U. H. (1999). Peridotite melting at 1.0 and 1.5 GPa: an experimental evaluation of techniques using diamond aggregates and mineral mixes for determination of near-solidus melts. Journal of Petrology, 40, 1343-1375.

Falloon, T. J., Green, D. H., O'Neill, H. S. C., and Hibberson, W. O. (1997). Experimental tests of low degree peridotite partial melt compositions: implications for the nature of anhydrous near-solidus peridotite melts at 1 GPa. Earth and Planetary Science Letters, 152, 149-162.

Filiberto, J. (2008). Experimental constraints on the parental liquid of the Chassigny meteorite: A possible link between the Chassigny meteorite and a Martian Gusev basalt. Geochimica et Cosmochimica Acta, 72, 690-701.

Filiberto, J. (2011). Geochemical differences between surface basalts and Martian meteorites: the need for Martian sample return. Lunar and Planetary Institute Contributions, 1611, 5004.

Filiberto, J., Chin, E., Day, J., Franchi, I. A., Greenwood, R. C., Gross, J., Penniston-Dorland, S. C., Schwenzer, S. P., and Treiman, A. H. (2012). Geochemistry of intermediate olivine-phyric shergottite Northwest Africa 6234, with similarities to basaltic shergottite Northwest Africa 480 and olivine-phyric shergottite Northwest Africa 2990. Meteoritics & Planetary Science, 47, 1256-1273.

Filiberto, J., and Dasgupta, R. (2011). Fe^{2+}–Mg partitioning between olivine and basaltic melts: Applications to genesis of olivine-phyric shergottites and conditions of melting in the Martian interior. Earth and Planetary Science Letters, 304, 527-537.

457 Filiberto, J., Jackson, C., Le, L., and Treiman, A. H. (2009). Partitioning of Ni between
458 olivine and an iron-rich basalt: Experiments, partition models, and planetary
459 implications. American Mineralogist, 94, 256-261.
460
461 Filiberto, J., and Treiman, A. H. (2009). The effect of chlorine on the liquidus of basalt:
462 First results and implications for basalt genesis on Mars and Earth. Chemical
463 Geology, 263, 60-68.
464
465 Filiberto, J., Treiman, A. H., and Le, L. (2008). Crystallization experiments on a Gusev
466 Adirondack basalt composition. Meteoritics & Planetary Science, 43, 1137-1146.
467
468 Gaetani, G. A., and Grove, T. L. (1998). The influence of water on melting of mantle
469 peridotite. Contributions to Mineralogy and Petrology, 131, 323-346.
470
471 Gee, L. L., and Sack, R. O. (1988). Experimental petrology of melilite
472 nephelinites. Journal of Petrology, 29, 1233-1255.
473
474 Goodrich, C. A. (2002). Olivine-phyric martian basalts: A new type of
475 shergottite. Meteoritics & Planetary Science, 37, B31-B34.
476
477 Greeley, R., Foing, B.H., McSween, H.Y., Neukum, G., Pinet, P., van Kan, M., Werner,
478 S.C., Williams, D.A., and Zegers, T.E. (2005) Fluid lava flows in Gusev crater, Mars.
479 Journal of Geophysical Research, 110, E05008, doi:10.1029/2005JE002401.
480

Greshake, A., Fritz, J., and Stöffler, D. (2004). Petrology and shock metamorphism of the olivine-phyric shergottite Yamato 980459: Evidence for a two-stage cooling and a single-stage ejection history. Geochimica et Cosmochimica Acta, 68, 2359-2377.

Gross, J., Treiman, A. H., Filiberto, J., & Herd, C. D. (2011). Primitive olivine-phyric shergottite NWA 5789: Petrography, mineral chemistry, and cooling history imply a magma similar to Yamato-980459. Meteoritics & Planetary Science, 46, 116-133.

Gross, J., Filiberto, J., Herd, C. D., Daswani, M. M., Schwenzer, S. P., and Treiman, A. H. (2013). Petrography, mineral chemistry, and crystallization history of olivine-phyric shergottite NWA 6234: A new melt composition. Meteoritics & Planetary Science, 48, 854-871.

Grove, T. L., and Bryan, W. B. (1983). Fractionation of pyroxene-phyric MORB at low pressure: an experimental study. Contributions to Mineralogy and Petrology, 84, 293-309.

Grove, T. L., Elkins-Tanton, L. T., Parman, S. W., Chatterjee, N., Müntener, O., and Gaetani, G. A. (2003). Fractional crystallization and mantle-melting controls on calc-alkaline differentiation trends. Contributions to Mineralogy and Petrology, 145, 515-533.

Grove, T. L., Gerlach, D. C., and Sando, T. W. (1982). Origin of calc-alkaline series lavas at Medicine Lake volcano by fractionation, assimilation and mixing. Contributions to Mineralogy and Petrology, 80, 160-182.

506 Grove, T. L., and Juster, T. C. (1989). Experimental investigations of low-Ca pyroxene
507 stability and olivine-pyroxene-liquid equilibria at 1-atm in natural basaltic and andesitic
508 liquids. Contributions to Mineralogy and Petrology, 103, 287-305.
509
510 Grove, T. L., Kinzler, R. J., and Bryan, W. B. (1992). Fractionation of mid-ocean ridge
511 basalt (MORB). Geophysical Monograph Series, 71, 281-310.
512
513 Herd, C.D.K. (2006). Insights into the redox history of the NWA 1068/1110 martian
514 basalt from mineral equilibria and vanadium oxybarometry. American Mineralogist, 91,
515 1616-1627.
516
517 Herd, C. D., Schwandt, C. S., Jones, J. H., and Papike, J. J. (2002). An experimental and
518 petrographic investigation of Elephant Moraine 79001 lithology A: Implications for its
519 petrogenesis and the partitioning of chromium and vanadium in a martian
520 basalt. Meteoritics & Planetary Science, 37, 987-1000.
521
522 Herzberg, C., Condie, K., and Korenega, J. (2010). Thermal history of the Earth and its
523 petrological expression. Earth and Planetary Science Letters, 292, 79-88.
524
525 Herzberg, C. and O'Hara, M.J. (1998). Phase equilibria constraints on the origin of
526 basalts, picrites, and komatites. Earth-Science Reviews, 44, 39-79.
527
528 Holbig, E. S., and Grove, T. L. (2008). Mantle melting beneath the Tibetan Plateau:
529 Experimental constraints on ultrapotassic magmatism. Journal of Geophysical
530 Research, 113, B04210.

Ikeda, Y. (2004). Petrology of the Yamato 980459 shergottite. Antarctic Meteorite Research, 17, 35.

Irving, A. J., Kuehner, S. M., Herd, C. D. K., Gellissen, M., Korotev, R. L., Puchtel, I., ... and Rumble, D. (2010). Petrologic, elemental and multi-isotopic characterization of permafic olivine-phyric shergottite Northwest Africa 5789: A primitive magma derived from depleted martian mantle. Lunar and Planetary Institute Science Conference, 41, 1547.

Jayasuriya, K. D., O'Neill, H. S. C., Berry, A. J., and Campbell, S. J. (2004). A Mössbauer study of the oxidation state of Fe in silicate melts. American Mineralogist, 89, 1597-1609.

Johnson, K. T. (1998). Experimental determination of partition coefficients for rare earth and high-field-strength elements between clinopyroxene, garnet, and basaltic melt at high pressures. Contributions to Mineralogy and Petrology, 133, 60-68.

Kennedy, A. K., Grove, T. L., and Johnson, R. W. (1990). Experimental and major element constraints on the evolution of lavas from Lihir Island, Papua New Guinea. Contributions to Mineralogy and Petrology, 104, 722-734.

Keshav, S., Gudfinnsson, G. H., Sen, G., and Fei, Y. (2004). High-pressure melting experiments on garnet clinopyroxenite and the alkalic to tholeiitic transition in ocean-island basalts. Earth and Planetary Science Letters, 223, 365-379.

Kiefer, W. S., Li, Q., and Filiberto, J. (2007). Parameterizations of magma production in a water-undersaturated martian mantle: A plea for improved experimental petrology constraints. In Workshop on Water in Planetary Basalts, 1, 22-23.

Kogiso, T., Hirose, K., and Takahashi, E. (1998). Melting experiments on homogeneous mixtures of peridotite and basalt: application to the genesis of ocean island basalts. Earth and Planetary Science Letters, 162, 45-61.

Kogiso, T., and Hirschmann, M. M. (2001). Experimental study of clinopyroxenite partial melting and the origin of ultra-calcic melt inclusions. Contributions to Mineralogy and Petrology, 142, 347-360.

Kogiso, T., Hirschmann, M. M., and Frost, D. J. (2003). High-pressure partial melting of garnet pyroxenite: possible mafic lithologies in the source of ocean island basalts. Earth and Planetary Science Letters, 216, 603-617.

Kress, V.C. and Carmichael, I.S. (1988). Stoichiometry of the iron oxidation reaction in silicate melts. American Mineralogist, 73, 1267-1274.

Kress, V.C. and Carmichael, I.S. (1991). The compressibility of silicate liquids containing Fe_2O_3 and the effect of composition, temperature, oxygen fugacity and pressure on their redox states. Contributions to Mineralogy and Petrology, 108, 82-92.

580 Laporte, D., Toplis, M. J., Seyler, M., and Devidal, J. L. (2004). A new experimental
581 technique for extracting liquids from peridotite at very low degrees of melting:
582 application to partial melting of depleted peridotite. Contributions to Mineralogy and
583 Petrology, 146, 463-484.
584
585 Lee, C. T. A., Luffi, P., Plank, T., Dalton, H., and Leeman, W. P. (2009). Constraints on
586 the depths and temperatures of basaltic magma generation on Earth and other terrestrial
587 planets using new thermobarometers for mafic magmas. Earth and Planetary Science
588 Letters, 279, 20-33.
589
590 Longhi, J., and Pan, V. (1989). The parent magmas of the SNC meteorites. Lunar and
591 Planetary Institute Science Conference, 19, 451-464.
592
593 Longhi, J., Walker, D., and Hays, J.F. (1978). The distribution of Fe and Mg between
594 olivine and lunar basaltic liquids. Geochmica et Cosmochimica Acta, 42, 1545-1558.
595
596 Matzen, A.K., Baker, M.B., Beckett, J.R., and Stolper, E.M. (2011). Fe-Mg partitioning
597 between olivine and high-magnesian melts and the nature of Hawaiian parental liquids.
598 Journal of Petrology, 52, 1243-1263.
599
600 McDade, P., Blundy, J. D., and Wood, B. J. (2003). Trace element partitioning on the
601 Tinaquillo Lherzolite solidus at 1.5 GPa. Physics of the Earth and Planetary
602 Interiors, 139, 129-147.
603

McCanta, M. C., Rutherford, M. J., and Jones, J. H. (2004). An experimental study of rare earth element partitioning between a shergottite melt and pigeonite: implications for the oxygen fugacity of the martian interior. Geochimica et Cosmochimica Acta, 68, 1943-1952.

McCallum, I. S., and Schwartz, J. M. (2001). Lunar Mg suite: Thermobarometry and petrogenesis of parental magmas. Journal of Geophysical Research, 106, 27969-27983.

McKay, G., Wagstaff, J., and Yang, S. R. (1986). Clinopyroxene REE distribution coefficients for shergottites: The REE content of the Shergotty melt. Geochimica et Cosmochimica Acta, 50, 927-937.

McCoy, T. J., and Lofgren, G. E. (1999). Crystallization of the Zagami shergottite: An experimental study. Earth and Planetary Science Letters, 173, 397-411.

McCubbin, F. M., Nekvasil, H., Harrington, A. D., Elardo, S. M., and Lindsley, D. H. (2008). Compositional diversity and stratification of the Martian crust: Inferences from crystallization experiments on the picrobasalt Humphrey from Gusev Crater, Mars. Journal of Geophysical Research, 113, E11013.

McSween, H. Y., Arvidson, R. E., Bell, J. F., Blaney, D., Cabrol, N. A., Christensen, P. R., ... and Zipfel, J. (2004). Basaltic rocks analyzed by the Spirit rover in Gusev Crater. Science, 305, 842-845.

628 Médard, E., and Grove, T. L. (2006). Early hydrous melting and degassing of the Martian
629 interior. Journal of Geophysical Research: Planets, 111, E11003.
630
631 Mikouchi, T., Koizumi, E., McKay, G., Monkawa, A., Ueda, Y., Chokai, J., and
632 Miyamoto, M. (2004). Yamato 980459: mineralogy and petrology of a new shergottite-
633 related rock from Antarctica. Antarctic Meteorite Research, 17, 13.
634
635 Minitti, M. E., and Rutherford, M. J. (2000). Genesis of the Mars Pathfinder "sulfur-free"
636 rock from SNC parental liquids. Geochimica et Cosmochimica Acta, 64, 2535-2547.
637
638 Monders, A. G., Médard, E., and Grove, T. L. (2007). Phase equilibrium investigations of
639 the Adirondack class basalts from the Gusev plains, Gusev crater, Mars. Meteoritics &
640 Planetary Science, 42, 131-148.
641
642 Musselwhite, D. S., Dalton, H. A., Kiefer, W. S., and Treiman, A. H. (2006).
643 Experimental petrology of the basaltic shergottite Yamato-980459: Implications for the
644 thermal structure of the Martian mantle. Meteoritics & Planetary Science, 41, 1271-1290.
645
646 Papike, J. J., Cameron, K. L., and Baldwin, K. (1974). Amphiboles and pyroxenes:
647 characterization of other than quadrilateral components and estimates of ferric iron from
648 microprobe data. In Geologic Society of America Abstract Programs, 6, 1053-1054.
649
650 Papike, J. J., Karner, J. M., Shearer, C. K., and Burger, P. V. (2009). Silicate mineralogy
651 of martian meteorites. Geochimica et Cosmochimica Acta, 73, 7443-7485.
652

653 Parman, S. W., Dann, J. C., Grove, T. L., and De Wit, M. J. (1997). Emplacement
654 conditions of komatiite magmas from the 3.49 Ga Komati Formation, Barberton
655 greenstone belt, South Africa. Earth and Planetary Science Letters, 150, 303-323.
656
657 Parman, S. W., and Grove, T. L. (2004). Harzburgite melting with and without H2O:
658 Experimental data and predictive modeling. Journal of Geophysical Research, 109,
659 B02201.
660
661 Pertermann, M., and Lundstrom, C. C. (2006). Phase equilibrium experiments at 0.5 GPa
662 and 1100–1300° C on a basaltic andesite from Arenal volcano, Costa Rica. Journal of
663 Volcanology and Geothermal Research, 157, 222-235.
664
665 Pichavant, M., Mysen, B. O., and MacDonald, R. (2002). Source and H2O content of
666 high-MgO magmas in island arc settings: an experimental study of a primitive calc-
667 alkaline basalt from St. Vincent, lesser antilles arc. Geochimica et Cosmochimica
668 Acta, 66, 2193-2209.
669
670 Putirka, K. D. (1998). Garnet+ liquid equilibrium. Contributions to Mineralogy and
671 Petrology, 131, 273-288.
672
673 Putirka, K. D. (2005). Mantle potential temperatures at Hawaii, Iceland, and the mid-
674 ocean ridge system, as inferred from olivine phenocrysts: Evidence for thermally driven
675 mantle plumes. Geochemistry, Geophysics, Geosystems, 6, 1-4.
676

677 Putirka, K. D. (2008). Thermometers and barometers for volcanic systems. Reviews in
678 Mineralogy and Geochemistry, 69, 61-120.
679
680 Putirka, K. D., Johnson, M., Kinzler, R., Longhi, J., and Walker, D. (1996).
681 Thermobarometry of mafic igneous rocks based on clinopyroxene-liquid equilibria, 0–30
682 kbar. Contributions to Mineralogy and Petrology, 123, 92-108.
683
684 Putirka, K. D., Mikaelian, H., Ryerson, F., and Shaw, H. (2003). New clinopyroxene-
685 liquid thermobarometers for mafic, evolved, and volatile-bearing lava compositions, with
686 applications to lavas from Tibet and the Snake River Plain, Idaho. American
687 Mineralogist, 88, 1542-1554.
688
689 Putirka, K. D., Perfit, M., Ryerson, F.J., and Jackson, M.G. (2007) Ambient and excess
690 mantle temperatures, olivine thermometry, and active vs. passive upwelling, Chemical
691 Geology, 241, 177-206.
692
693 Putirka, K.D., Ryerson, F.J., Perfit, M., and Ridley, W.I. (2011) Mineralogy and
694 composition of the oceanic mantle, Journal of Petrology, 52, 279-313.
695
696 Roeder, P. L., and Emslie, R. (1970). Olivine-liquid equilibrium. Contributions to
697 Mineralogy and Petrology, 29, 275-289.
698
699 Robinson, J. A. C., Wood, B. J., and Blundy, J. D. (1998). The beginning of melting of
700 fertile and depleted peridotite at 1.5 GPa. Earth and Planetary Science Letters, 155, 97-
701 111.

SAS Institute Inc. (2010). JMP. Version 9.0.1, Cary, NC

Schwab, B. E., and Johnston, A. D. (2001). Melting systematics of modally variable, compositionally intermediate peridotites and the effects of mineral fertility. Journal of Petrology, 42, 1789-1811.

Singletary, S. J., and Grove, T. L. (2008). Experimental petrology of the Mars Pathfinder rock composition: Constraints on the interpretation of Martian reflectance spectra. Journal of Geophysical Research, 113, E11011.

Takahahshi, E., Nakajima, K., and Wright, T. L. (1998). Origin of the Columbia River basalts: melting model of a heterogeneous plume head. Earth and Planetary Science Letters, 162, 63-80.

Toplis, M.J. (2005). The thermodynamics of iron and magnesium partitioning between olivine and liquid: criteria for assessing and predicting equilibrium in natural and experimental systems. Contributions to Mineralogy and Petrology, 149, 22-39.

Tsuruta, K., and Takahashi, E. (1998). Melting study of an alkali basalt JB-1 up to 12.5 GPa: behavior of potassium in the deep mantle. Physics of the Earth and Planetary Interiors, 107, 119-130.

Usui, T., McSween Jr, H. Y., and Floss, C. (2008). Petrogenesis of olivine-phyric shergottite Yamato 980459, revisited. Geochimica et Cosmochimica Acta, 72, 1711-1730.

Villiger, S., Ulmer, P., Müntener, O., and Thompson, A. B. (2004). The liquid line of descent of anhydrous, mantle-derived, tholeiitic liquids by fractional and equilibrium crystallization—an experimental study at 1.0 GPa. Journal of Petrology, 45, 2369-2388.

Walter, M. J. (1998). Melting of garnet peridotite and the origin of komatiite and depleted lithosphere. Journal of Petrology, 39, 29-60.

Werner, S.C., Ody, A., and Poulet, F. (2014). The source crater of martian shergottite meteorites. Science, 343, 1343-1346.

Figure Captions

Figure 1. Comparison of basaltic liquid compositions between martian and terrestrial compositions (in weight %). These comparisons show distinct compositional differences. Grey crosses represent terrestrial samples while black circles represent martian samples. Martian data sources are outlined in Table 4 and terrestrial data sources are from: Bulatov et al. (2002), Draper and Green (1997, 1999), Draper and Johnston (1992), Dunn and Sen (1994), Elkins-Tanton and Grove (2003), Elkins-Tanton et al. (2007), Falloon et al. (1997, 1999, 2001), Gaetani and Grove (1998), Gee and Sack (1988), Grove et al. (1982), Grove and Bryan (1983), Grove and Juster (1989), Grove et al. (1992), Grove et al. (2003), Holbig and Grove (2008), Johnson (1998), Kennedy et al. (1990), Keshav et al.

(2004), Kogiso and Hirschmann (2001), Kogiso et al. (1998, 2003), Laporte et al. (2004), McDade et al. (2003), Parman et al. (1997), Parman and Grove (2004), Pertermann and Lundstrom (2006), Pichavant et al. (2002), Putirka (1998), Putirka et al. (1996, 2003), Robinson et al. (1998), Schwab and Johnston (2001), Takahahshi et al. (1998), Tsuruta and Takahashi (1998), Villiger et al. (2004), and Walter (1998).

Figure 2. Pressures in GPa recovered from model 1. The data are separated into calibration data (open gray circles) and test data (closed black circles). A one-to-one correlation line is presented as the dashed gray line.

Figure 3 Temperatures in K recovered from model 2. The data are separated into calibration data (open gray circles) and test data (closed black circles). A one-to-one correlation line is presented as the dashed gray line.

Figure 4. Pressures in GPa recovered from model 3. The data are separated into calibration data (open gray circles) and test data (closed black circles). A one-to-one correlation line is presented as the dashed gray line.

Figure 5. Temperatures in K recovered from model 4. The data are separated into calibration data (open gray circles) and test data (closed black circles). A one-to-one correlation line is presented as the dashed gray line.

Figure 6. Temperatures in K recovered from model 5. The data are separated into calibration data (open gray circles) and test data (closed black circles). Hydrated calibration data is shown in closed grey circles while hydrated test data is presented as a

775 closed black square. Cl-rich calibration data is shown in closed grey diamonds and Cl-
776 rich test data is presented as a closed black diamond. A one-to-one correlation line is
777 presented as the dashed gray line.
778
779 **Figure 7.** Pressures in GPa recovered from model 6. The data are separated into
780 calibration data (open gray circles) and test data (closed black circles). A one-to-one
781 correlation line is presented as the dashed gray line.
782
783 **Figure 8.** Temperatures in K recovered from model 7. The data are separated into
784 calibration data (open gray circles) and test data (closed black circles). A one-to-one
785 correlation line is presented as the dashed gray line.
786
787 **Figure 9.** Pressures in GPa recovered from model 8. The data are separated into
788 calibration data (open gray circles) and test data (closed black circles). A one-to-one
789 correlation line is presented as the dashed gray line.
790
791 **Figure 10.** The Si-Activity barometer (Eqn. 8) is combined with the olivine thermometer
792 (Eqn. 5) (grey symbols) and then with the empirical MgO thermometer (Eqn. 17) (black
793 symbols) to produce pressures and temperatures for Y98459 (closed circles), NWA 6234
794 (closed squares), NWA 1068 (closed diamonds), and a martian surface basalt (Gusev)
795 (closed triangle) using sample data from Greshake et al (2004), Gross et al (2013),
796 McSween (2004), and Monders et al. (2007) respectively. Our models are compared to *P*-
797 *T* conditions found in: Musselwhite et al. (2006), Blinova and Herd (2009), and Lee et al.
798 (2009) for Y98 (open circles); Gross et al. (2013) for NWA 6234 (open square); and

799 Monders et al. (2007) for the Gusev basalt (open triangle). The grey line represents the
800 martian mantle solidus, estimated from Kiefer et al. (2007).
801
802 **Tables**
803
804 **Table 1.** Experimental studies on martian meteorites and their analogs used in this study.
805 Shown in this table are their respective pressure and temperature ranges as well as their
806 mineral phases.

Source	Pressure Ranges (GPa)	Temperature Ranges (˚C)	Cpx	Opx	Ol
Bertka and Holloway (1987)	2.3	1400-1440	X	X	X
Dann et al. (2001)	0.0001-0.2	960-1175	X	X	X
Filberto and Treiman (2009)	0.57-1.17	1200-1315		X	X
Filberto et al. (2008)	0.0001-1.57	1200-1385		X	X
Filberto et al. (2009)	0.77-1.37	1300-1390		X	X
Filberto et al. (2010)	0.01-2.07	1390-1520		X	X
Filberto (2008)	0.43-0.93	972-1232	X	X	X
Herd et al. (2002)	0.0001	1150-1250	X		X
Longhi and Pan (1989)	0.0001013	1215-1300	X		X
McCanta et al. (2004)	0.0001013-0.02	1110-1165		X	
McCay et al. (1986)	0.0001013	1140-1171	X	X	
McCoy and Lofgren (1999)	0.0001013	1050-1175	X	X	
McCubbin et al. (2008)	0.93	1100-1250	X	X	X
Medard and Grove (2006)	1.0-1.5	975-1000	X	X	
Minitti and Rutherford (2000)	0.0001-0.02	950-1130	X	X	
Monders et al. (2007)	0.0001-1.55	1105-1360		X	X

Musselwhite et al. (2006)	0.45-1.38	1410-1540			X
Singletary and Grove (2008)	0.0001-0.1	950-1050	X		

807

808 **Table 2.** A summary of useful statistic for the models created in this study separated into
809 calibration and test data results for each model. The statistics in this table were
810 calculated by JMP statistical software version 9.0.1.

811

Model	**R^2**	**RMSE**	**n**
Clinopyroxene+Liquid			
1) Calibration	0.91	0.17 GPa	42
Test	0.94	0.22 GPa	9
2) Calibration	0.96	22 K	42
Test	0.90	41 K	9
Orthopyroxene+Liquid			
3) Calibration	0.89	0.20 GPa	75
Test	0.91	0.21 GPa	14
4) Calibration	0.94	33 K	74
Test	0.96	27 K	14
Olivine+Liquid			
5) Calibration	0.88	48 K	95
Test	0.90	38 K	20
Two-Pyroxene			
6) Calibration	0.93	0.17 GPa	31
Test	0.96	16 GPa	8
7) Calibration	0.99	12 K	24

Test	0.95	37 K	5
Si-Activity			
8) Calibration	0.91	0.16 GPa	22
Test	0.92	18 GPa	7

812

813 **Table 3.** A summary of useful statistic for the previously published models from Putirka
814 et al. (1996) and Putirka (2008) when applied to the same experimental martian meteorite
815 data used in the creation of the models in this study. The statistics in this table were
816 calculated in JMP statistical software version 9.0.1. Pressures in GPa have been
817 converted from their original units of kbar.

818

Model	**R^2**	**RMSE**	**n**
Clinopyroxene+Liquid			
Puritka (2008) Eq. 32a	0.55	0.40 Gpa	59
Putirka et al. (1996) Eq. T1	0.76	52 K	50
Orthopyroxene+Liquid			
Puritka (2008) Eq. 29c	0.22	0.59 GPa	32
Two-Pyroxene			
Putirka (2008) Eq. 38	0.08	0.62 GPa	39
Putirka (2008) Eq. 36	0.49	75 °C	39
Si-Activity			
Putirka (2008) Eq. 42	0.81	0.24 GPa	29

819

820 **Figures**

821 **Figure 1.**

Figure 2.

Figure 3.

Figure 4.

Figure 5.

Figure 6.

Figure 7.

Figure 8.

Figure 9.

Figure 10.

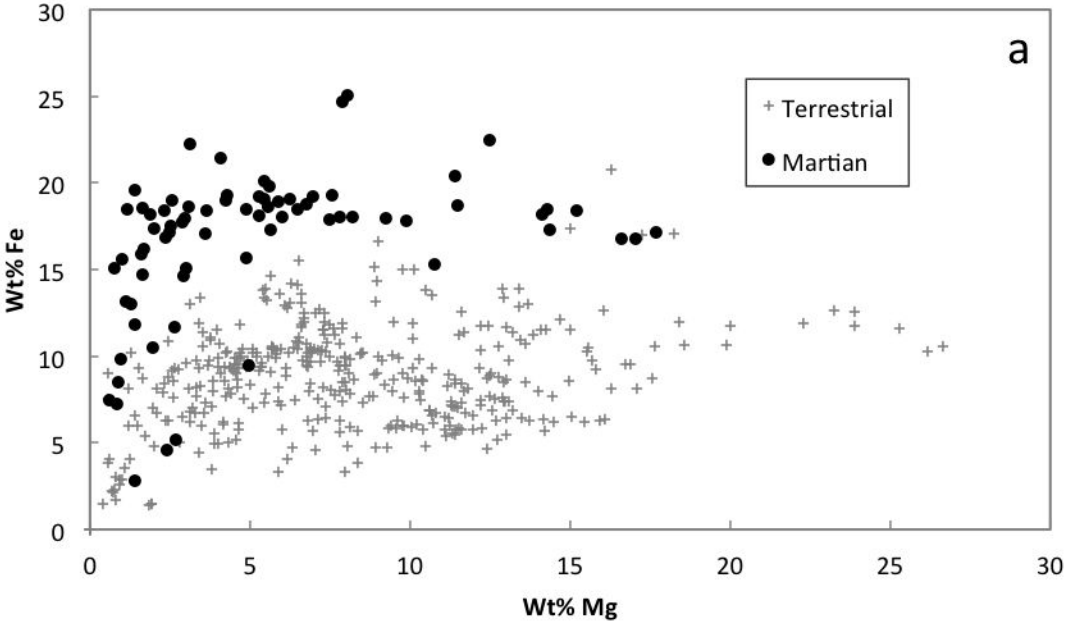
a
Terrestrial
Martian
Wt% Fe
Wt% Mg
0
5
10
15
20
25
30

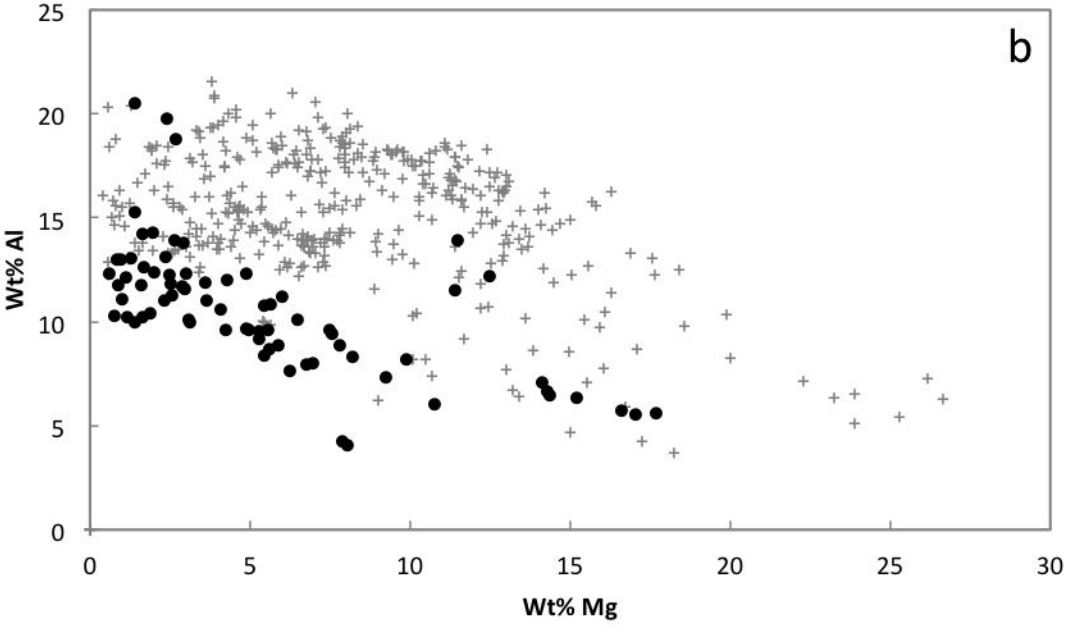
b
Wt% Al
Wt% Mg
0
5
10
15
20
25
30

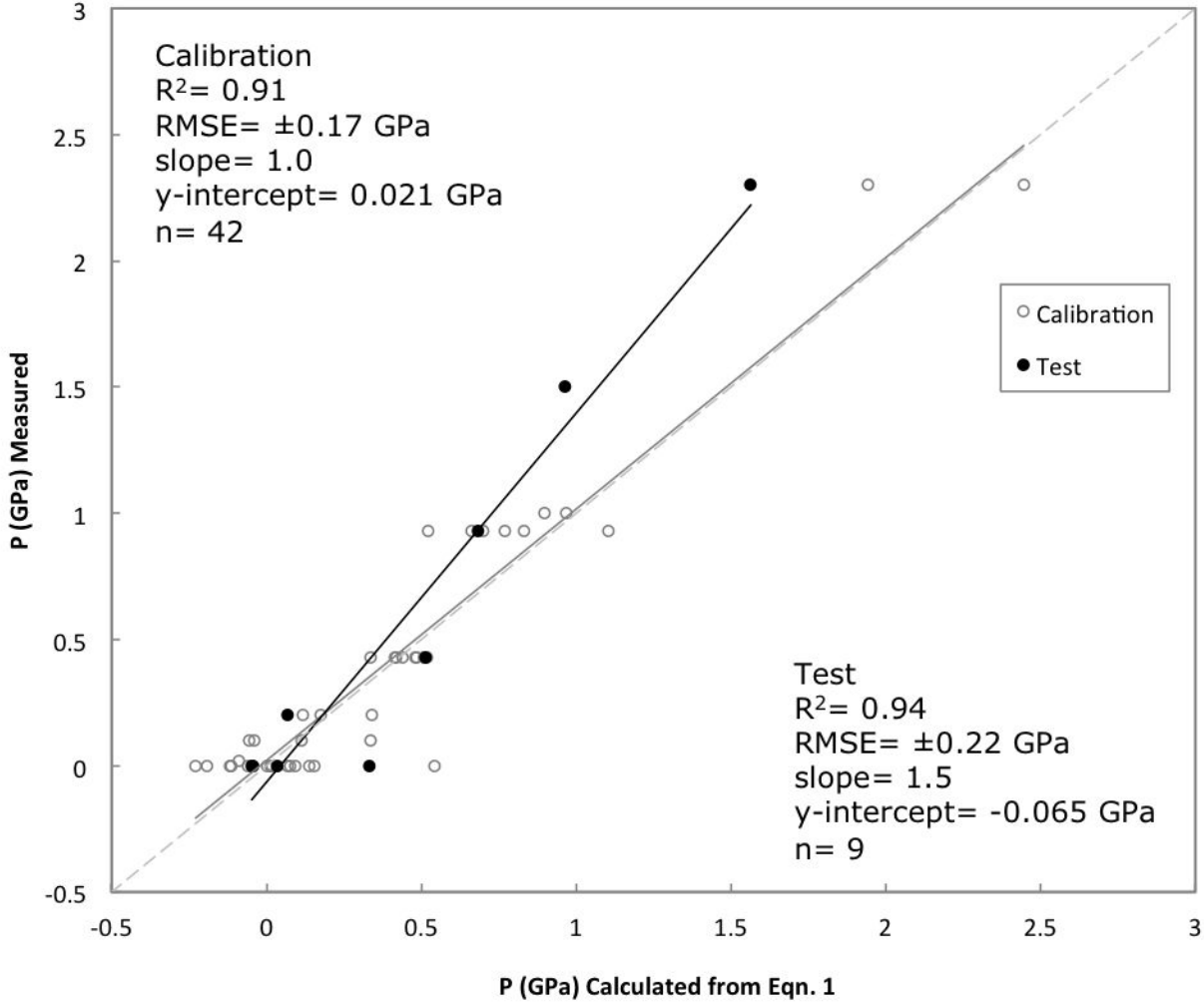
Calibration
R2= 0.91
RMSE= ±0.17 GPa
slope= 1.0
y-intercept= 0.021 GPa
n= 42
Test
R2= 0.94
RMSE= ±0.22 GPa
slope= 1.5
y-intercept= -0.065 GPa
n= 9
Calibration
Test
P (GPa) Measured
P (GPa) Calculated from Eqn. 1
3
2.5
2
1.5
1
0.5
0
-0.5
-0.5
0
0.5
1
1.5
2
2.5
3

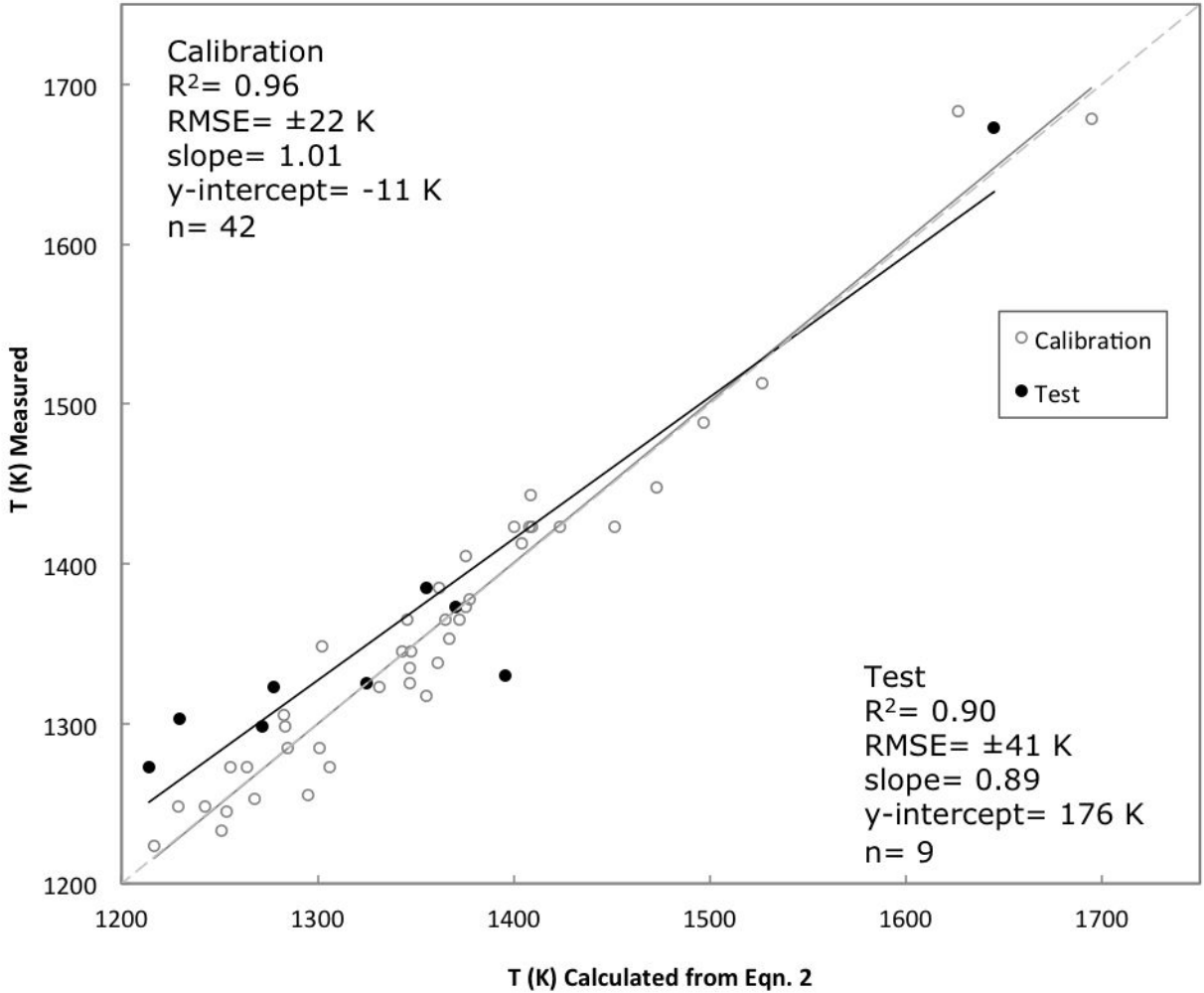
Calibration
R2= 0.96
RMSE= ±22 K
slope= 1.01
y-intercept= -11 K
n= 42
Test
R2= 0.90
RMSE= ±41 K
slope= 0.89
y-intercept= 176 K
n= 9
Calibration
Test
T (K) Measured
T (K) Calculated from Eqn. 2
1200
1300
1400
1500
1600
1700

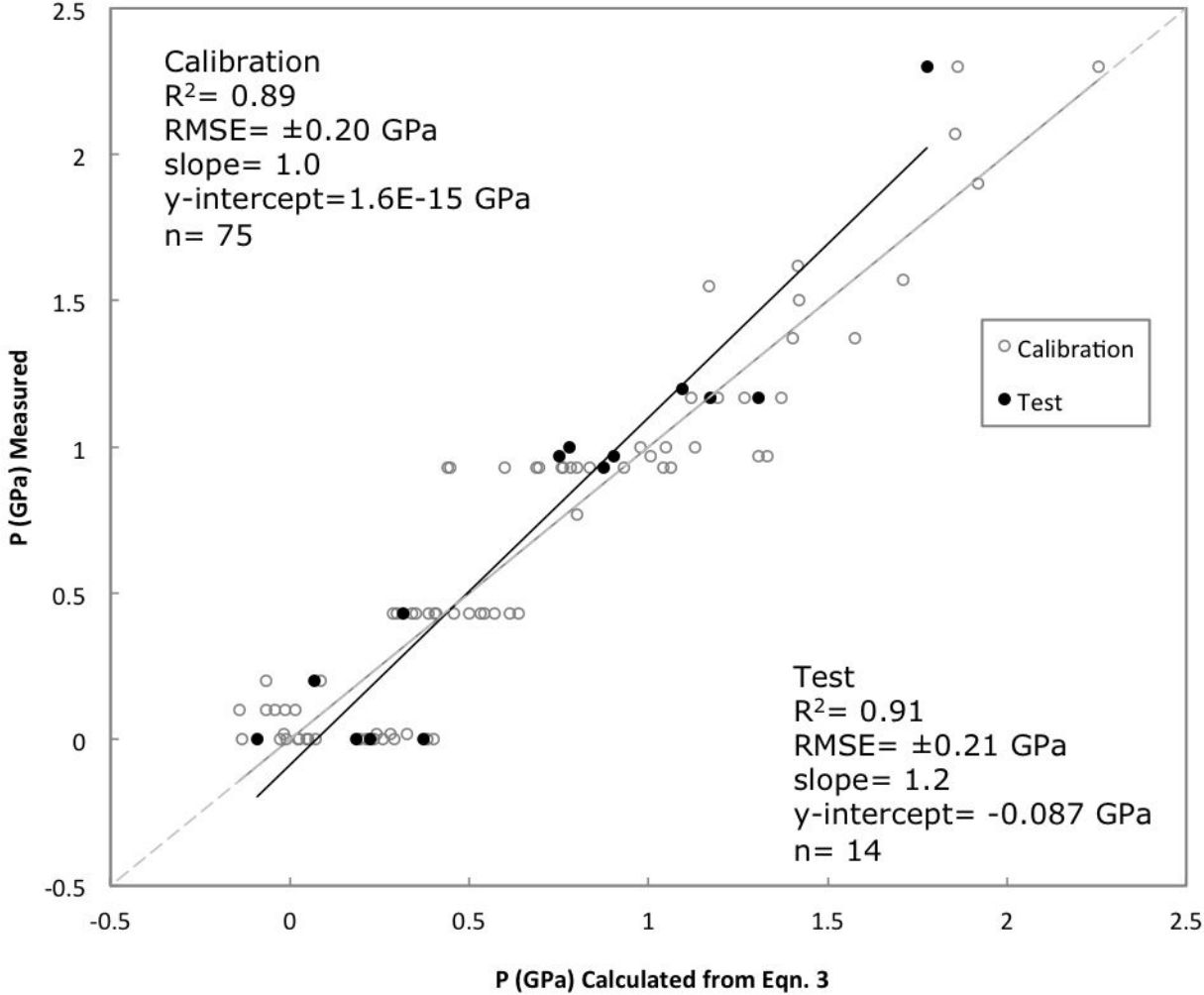
Calibration
R2= 0.89
RMSE= ±0.20 GPa
slope= 1.0
y-intercept=1.6E-15 GPa
n= 75
Calibration
Test
Test
R2= 0.91
RMSE= ±0.21 GPa
slope= 1.2
y-intercept= -0.087 GPa
n= 14
P (GPa) Measured
P (GPa) Calculated from Eqn. 3
2.5
2
1.5
1
0.5
0
-0.5
-0.5
0
0.5
1
1.5
2
2.5

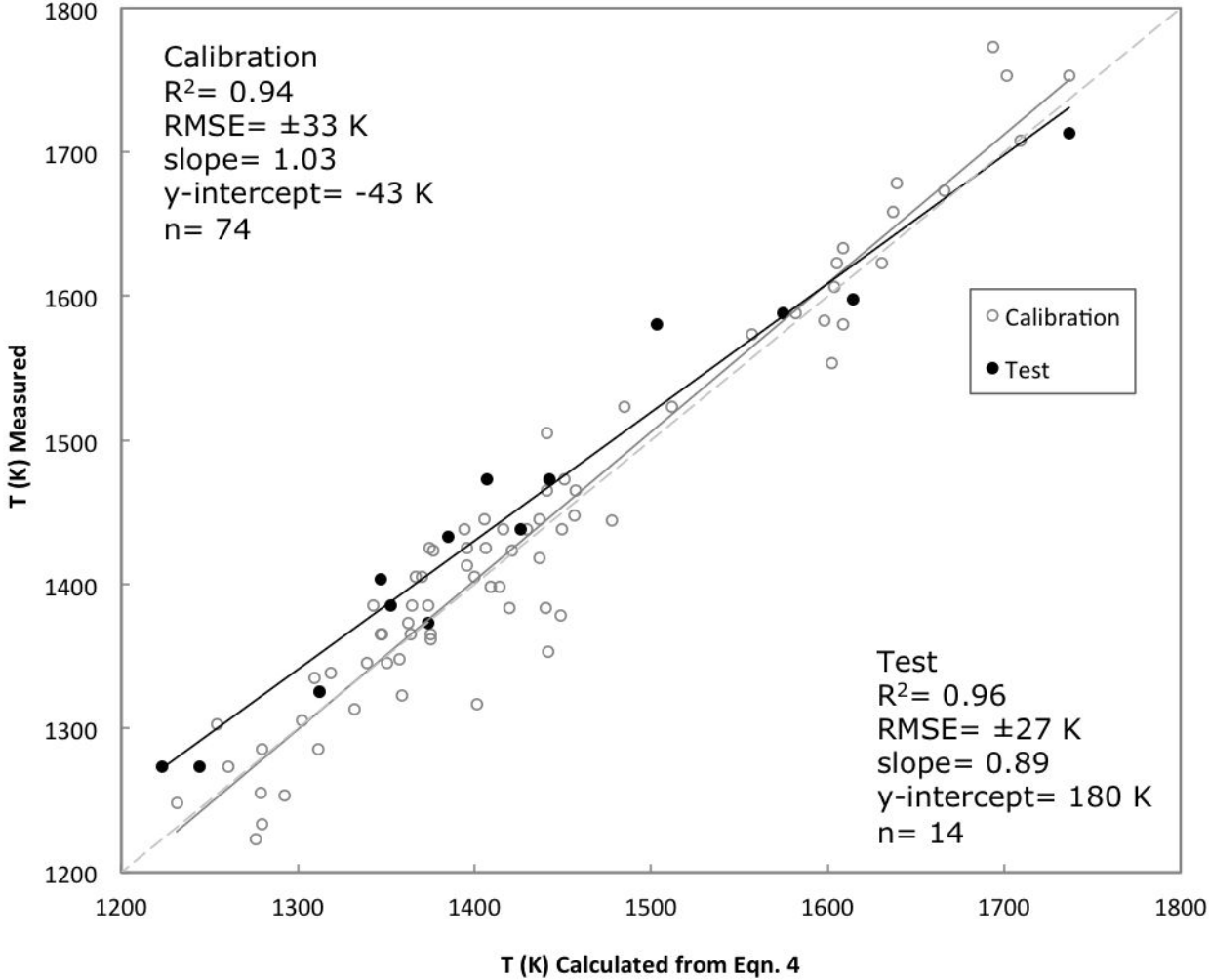
Calibration
R²= 0.94
RMSE= ±33 K
slope= 1.03
y-intercept= -43 K
n= 74
Calibration
Test
Test
R²= 0.96
RMSE= ±27 K
slope= 0.89
y-intercept= 180 K
n= 14
T (K) Measured
T (K) Calculated from Eqn. 4
1800
1700
1600
1500
1400
1300
1200
1200
1300
1400
1500
1600
1700
1800

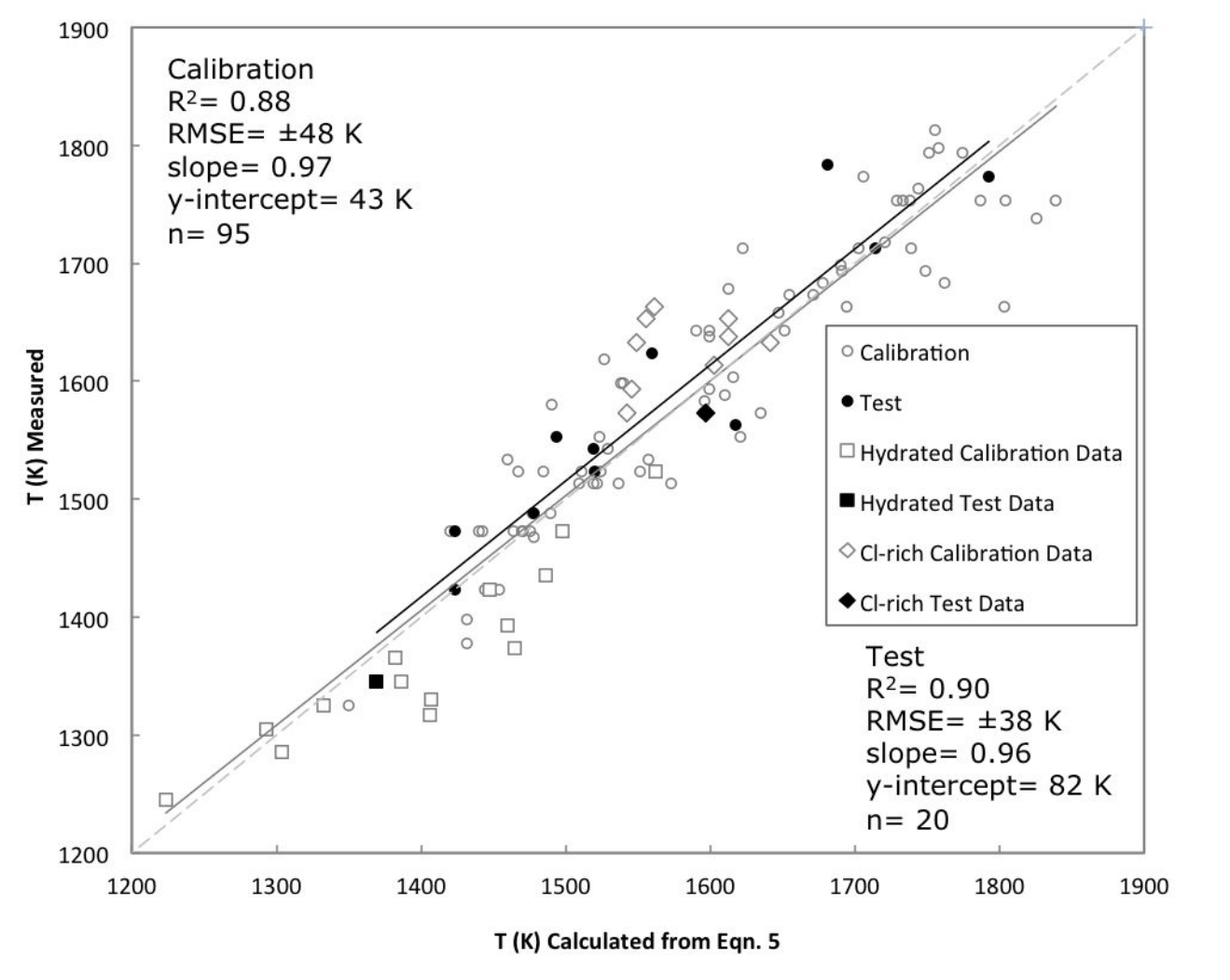
Calibration
R2= 0.88
RMSE= ±48 K
slope= 0.97
y-intercept= 43 K
n= 95
Test
R2= 0.90
RMSE= ±38 K
slope= 0.96
y-intercept= 82 K
n= 20
Calibration
Test
Hydrated Calibration Data
Hydrated Test Data
Cl-rich Calibration Data
Cl-rich Test Data
T (K) Measured
T (K) Calculated from Eqn. 5
1200
1300
1400
1500
1600
1700
1800
1900

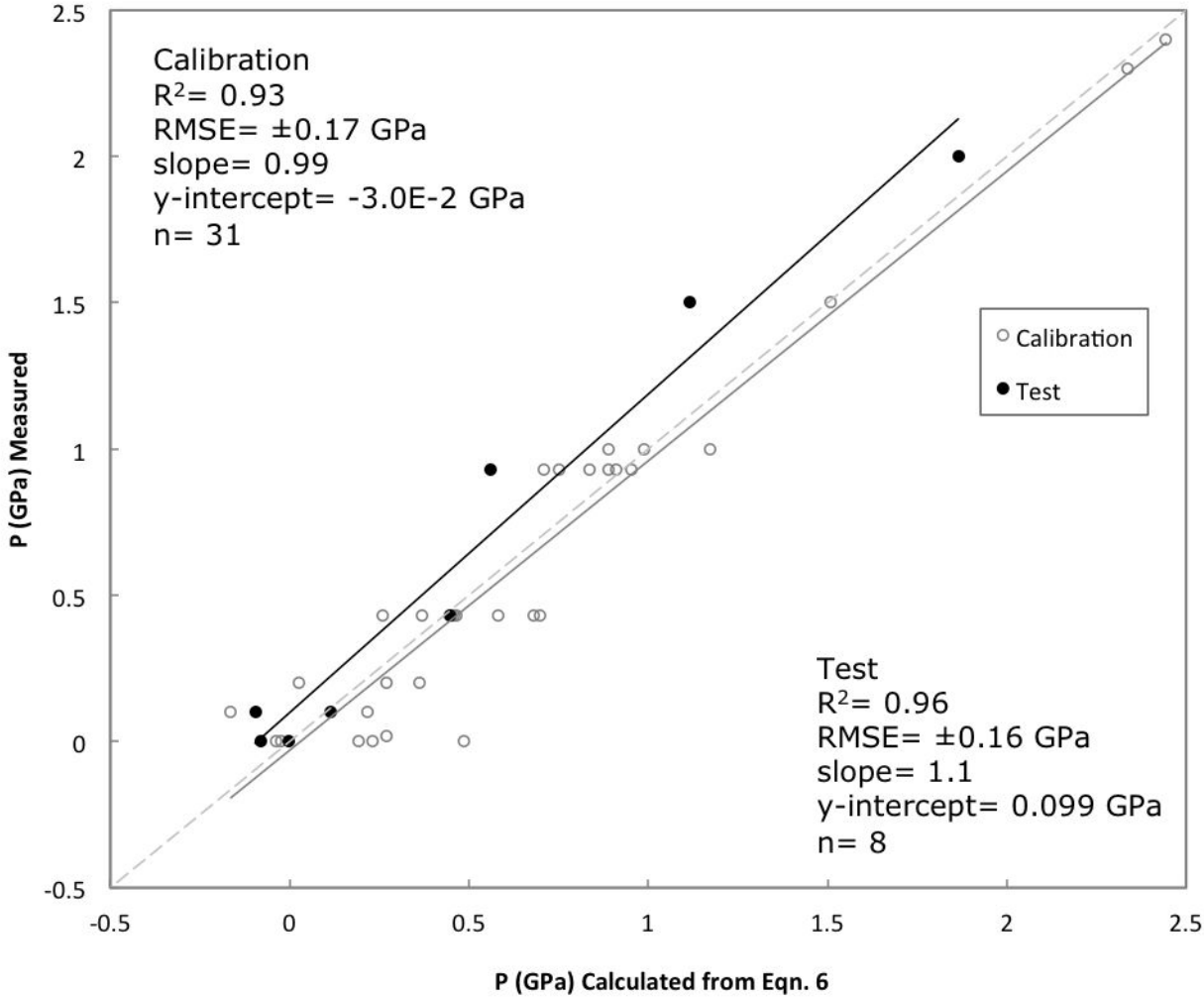
Calibration
R2= 0.93
RMSE= ±0.17 GPa
slope= 0.99
y-intercept= -3.0E-2 GPa
n= 31
Test
R2= 0.96
RMSE= ±0.16 GPa
slope= 1.1
y-intercept= 0.099 GPa
n= 8
Calibration
Test
P (GPa) Measured
P (GPa) Calculated from Eqn. 6
2.5
2
1.5
1
0.5
0
-0.5
-0.5
0
0.5
1
1.5
2
2.5

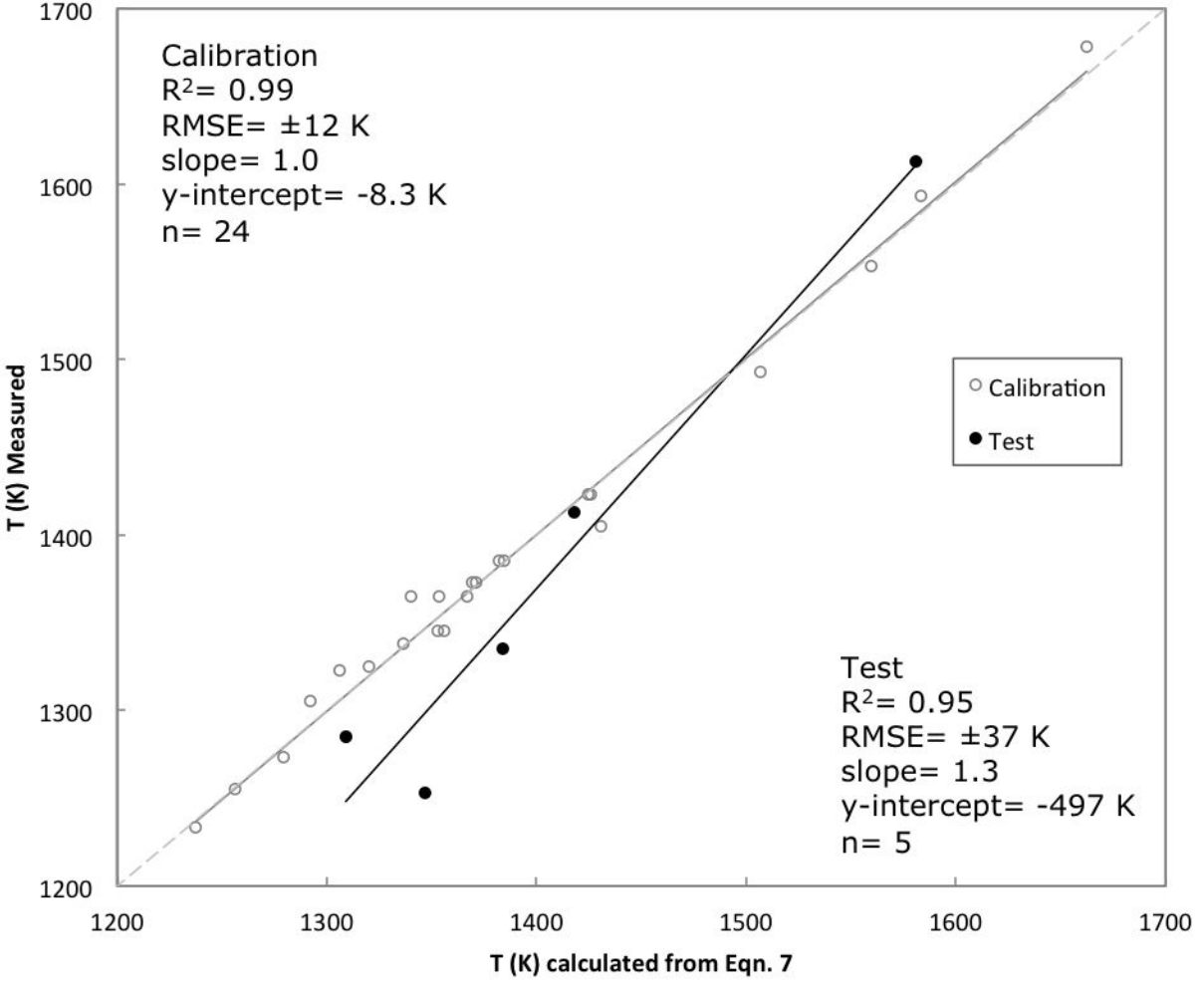
Calibration
R2= 0.99
RMSE= ±12 K
slope= 1.0
y-intercept= -8.3 K
n= 24
Test
R2= 0.95
RMSE= ±37 K
slope= 1.3
y-intercept= -497 K
n= 5
Calibration
Test
T (K) Measured
T (K) calculated from Eqn. 7
1200
1300
1400
1500
1600
1700

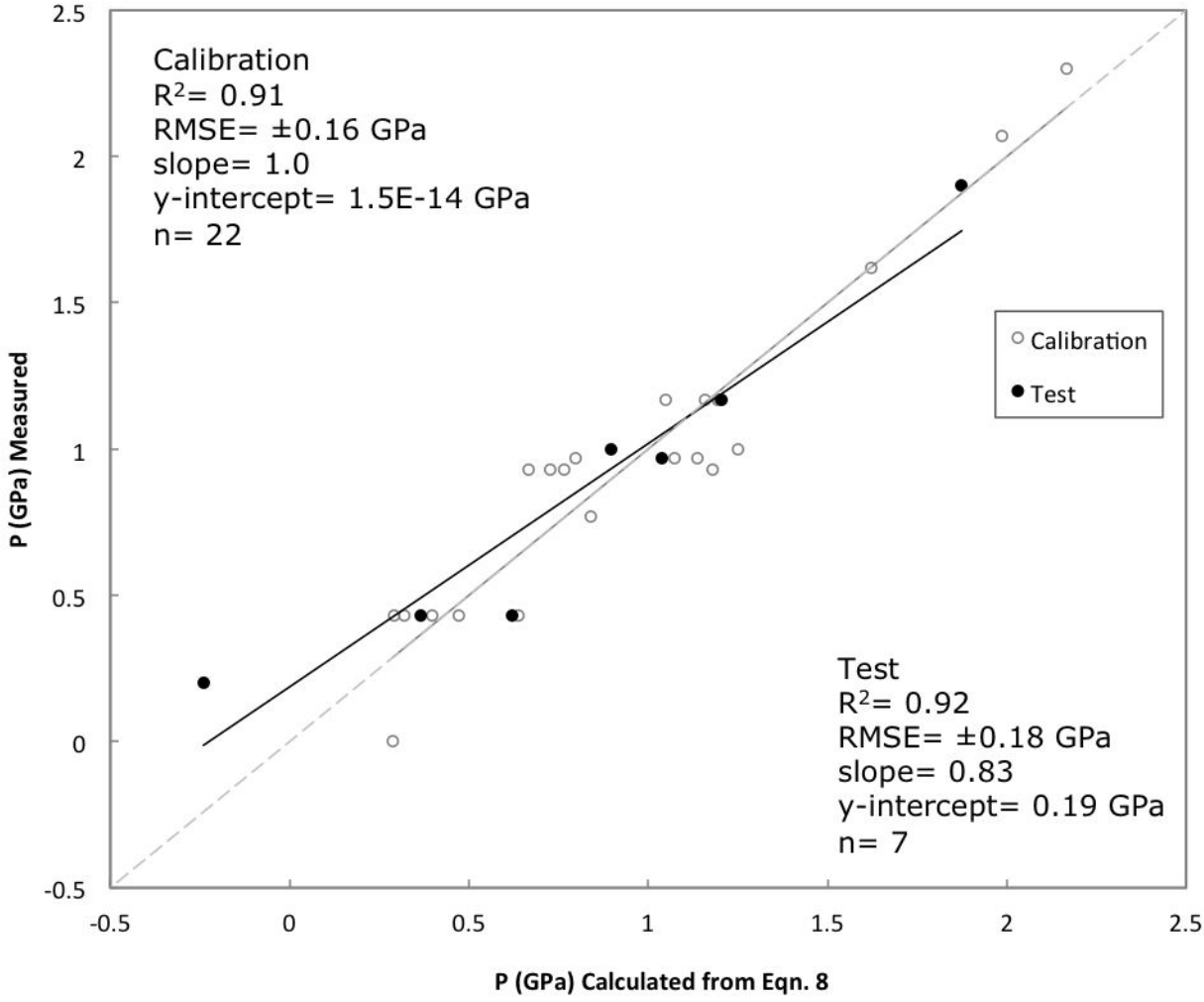
Calibration
R²= 0.91
RMSE= ±0.16 GPa
slope= 1.0
y-intercept= 1.5E-14 GPa
n= 22
Test
R²= 0.92
RMSE= ±0.18 GPa
slope= 0.83
y-intercept= 0.19 GPa
n= 7
Calibration
Test
P (GPa) Measured
P (GPa) Calculated from Eqn. 8
2.5
2
1.5
1
0.5
0
-0.5
-0.5
0
0.5
1
1.5
2
2.5

Temperature (°C)

1250 1300 1350 1400 1450 1500 1550 1600 1650

Pressure (GPa)

0 0.5 1 1.5 2 2.5 3

Y980 This work, Ol and Si-act (Equations 17 and 8)

Y980 This work, Ol and Si-act (Equations 5 and 8)

Y980 estimates from previous authors

NWA 6234 This work Ol and Si-act (Equations 17 and 8)

NWA 6234 This work, Ol and Si-act (Equations 5 and 8)

NWA 6234 Gross et al., 2013

NWA 1068 This work, Ol and Si-act (Equations 17 and 8)

NWA 1068 This work, Ol and Si-act (Eqiuations 5 and 8)

Gusev basalt this work, Ol and Si-act (Equations 17 and 8)

Gusev basalt this work, Ol and Si-act (Equations 5 and 8)

Gusev basalt Monders et al. 2007

Solidus from Kiefer et al., 2007